UNIVERSITE DE NICE - SOPHIA ANTIPOLIS - UFR Sciences
Ecole doctorale << Sciences fondamentales et appliquées >>

THESIS

for the title of
Docteur en Sciences
de l'université de Nice-Sophia Antipolis
Discipline: Sciences de l'Univers

Sandrine THOMAS

Study of an adaptive optics for the astronomy in the visible

WFS study part

Thesis directed by **Andrei TOKOVININ**

Jury

M. Renaud FOY	Rapporteur
M. Gérard ROUSSET	Rapporteur
M. Jean-Luc BEUZIT	Examinateur
M. Thierry FUSCO	Examinateur
M. Farrokh VAKILI	Examinateur

Part I

Optimization of an adaptive optic system

Chapter I.1

Study of an wavefront sensor: The Shack-Hartmann

I.1.1 Introduction

In this chapter, I present a study of the Shack-Hartmann wavefront sensor (SH). The goal is to optimize the slopes measurement in the SH, thus the wavefront deformation, to get better performance of a given adaptive optics (AO). The main conclusion of this study is that there is no miracle solution for all AO, but the best algorithm depends on the AO considered.
Three main problem are highlighted in this study:
- Detectability at low flux. In a "classical" AO using a natural guide star, the number of photons on the CCD is low. Therefore, even with low readout noise, there is a problem of signal detectability against the noise and trustability of the measurements;
- Noise propagation in presence of medium flux;
- Saturation and/or linearity problem at high flux especially in open loop.

In this part, I first describe the context and the different centroid algorithms such as the center of gravity (CoG), the windowing and thresholding, the weighted center of gravity (WCoG) and correlation. In a second part, I present the optimization of those methods, first without any atmospherical turbulence (Gaussian or diffraction limiter spot) and then with atmospherical turbulence. In addition, the paper describes two special cases: the Planet Finder and the SOAR AO, SAM.

In this report, I will only consider one square sub-aperture. Its dimensions are $d \times d$ (m). The region of interest on the CCD is $W_{fov} \times W_{fov}$ (λ/d).

I.1.2 Problem description

It is necessary to precisely measure the spot position on a SH. Table I.1.1 gathers all the parameters and notations used in the study.

Table I.1.1: List of parameters and notations

Notation	Parameter	Value	Unit
N_{ph}	Number of photons per subaperture and frame	$[30, 10000]$	photons
N_r	Readout noise per pixel and frame	$[0, 3]$	électrons
SNR	Signal to noise ratio = N_{ph}/N_r		
$I(x, y)$	Image intensity at the pixel (x,y)		photons
$N_{tot} \times N_{tot}$	Dimension of the calculation window	<32×32	pixels
Dep_{amp}	Spot motion amplitude rms	0.1	pixels
N_T	FWHM of the image spot	[1-2]	pixels
σ	Spot size rms		pixels
	$\frac{N_{samp}}{2\sqrt{2ln(2)}}$ for a Gaussian spot	0.85	pixels
N_{samp}	FWHM of the diffracted spot	[1-2]	pixels
p	Pixel size(=$(\lambda/d)/N_{samp}$)		rad
$d \times d$	Subaperture size	0.4	meter
λ	Wavelength		microns
$W_{fov} \times W_{fov}$	Subaperture field of view	<16×16	λ/d
r_0	Fried diameter	$[d/5, 2 * d]$	meter
T	Percentage of the maximum defining the threshold value in the thresholding method	0.2	
$W \times W$	Region of calculation in the windowing method	[4-32]	pixels
$P(x, y)$	Reference function, Gaussian		
$I_c(x, y)$	Correlation function		photons^2
n	"Oversampling" factor of the correlation	[1-4]	
$N_c \times N_c$	Size window for the correlation	n*[16-64]	pixels
$W_c \times W_c$	region of calculation of the correlation peak	[3-32]	pixels
N_w	FWHM of the reference function		pixels
K_s	Factor defining N_w such as $N_w = K_s N_{samp}$	[1-16]	
δ	FWHM of the I_c		pixels
T_{corr}	Percentage of the maximum defining the threshold value for I_c peak determination by CoG		
$\sigma^2_{\Delta\phi}$	Phase error variance		radians^2
D_x, D_y	Know center of mass	[-0.5,0.5]	pixels
$(C_{mes})_x, (C_{mes})_y$	Measured center of mass		pixels
α	Response coefficient		

Comments:

- The window size is expressed either in pixels or in λ/d, where λ/d is the size of the diffraction spot produced by the subaperture. Three spot shapes have been studied: Gaussian spot, diffraction spot, diffraction spot distorted by the turbulence. For all three cases, the pixel size and the FoV size are relative to λ/d.

- Signal to noise ration definition (SNR): the SNR can have several definitions. In this report, I use SNR for $SNR = N_{ph}/N_r$, where N_{ph} is the mean number of photons per subaperture and frame and N_r the readout noise per pixel and frame.

I.1.2.1 Noise

The noise term gathers readout noise, photon noise, and noise due to the atmospherical turbulence. Fig. I.1.1, I.1.2, I.1.3 show the images obtained at the focal plane of a square lenslet in the case of a perfect wavefront – figure I.1.1 –, for a wavefront distorted by atmospherical turbulence – figure I.1.2 –, and finally for a wavefront distorted by atmospherical turbulence in presence of readout noise and photon noise – figure I.1.3. All the spot are Nyquist sampled.

From those images, it is obvious that the centroid calculation will be affected by those different noise. The goal is to find a algorithm that ***minimizes the noise propagation***, ***linear*** and ***robust***.

- **Good noise propagation:** to minimize the noise impact on the CoG calculation. We will adjust the parameters (T, W, T_{corr}...) to decrease the noise variance. It is important to note that this is not the propagation noise in the OA system but only the noise propagation to the spot position determination;
- **Linearity and response coefficient:** we want to get an unbiased measure meaning that for a spot motion D_x, I measure the same motion D_x and not αD_x where $\alpha < 1$. Moreover, we want to get a linear response. Therefore, if the measured spot position is written $(C_{mes})_x = \alpha D_x + \beta$, where β is the non-linearity coefficient, we want $alpha = 1$ and $\beta = 0$.
- **Robustness** when the SNR is low, the reliability of the measurement is low. One way to overcome this limitation is to disregard the measures that are a priori false. (cf section I.1.4.2).

I.1.2.2 Merit function

The parameter to evaluate the performance is the error variance σ_{err}, calculated from the error made on the spot position estimation. σ_{err} is in $pixels^2$:

$$\sigma^2_{err} = \langle (C_{mes} - D_x)^2 \rangle, \tag{I.1.1}$$

where D_x is the true value of the center of mass, C_{mes} is the measured value of the center of mass and $\langle . \rangle$ is the classical mean.

The parameters varying in this study are:

- the number of photons or the SNR (c.f. section I.1.2) in presence of readout noise;
- d/r_0 to quantify the amount of atmospherical turbulence;
- the parameters of each algorithm: T and T_{corr}, N_w.

The general expression of the position estimator is

$$C_{mes} = \alpha D_x + f_{nl}(D_x) + \epsilon + noise, \tag{I.1.2}$$

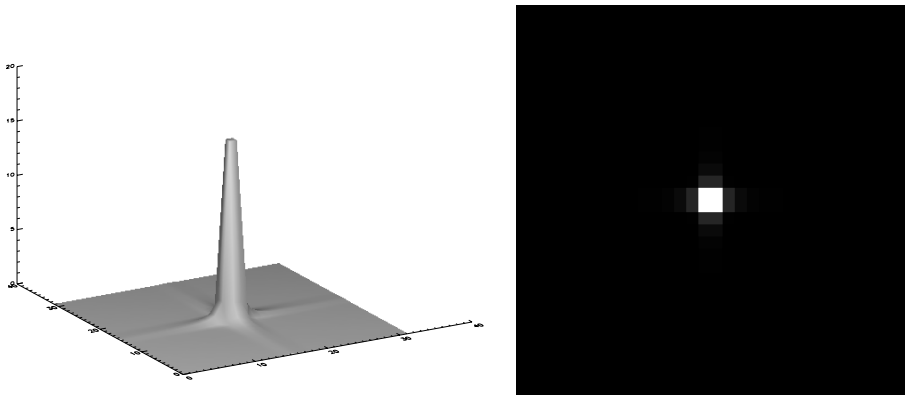

Figure I.1.1: diffraction spot at the lenslet focal plane. The subaperture is square with a FoV of 16×16 λ/d. The wavefront is perfect and there is no noise.

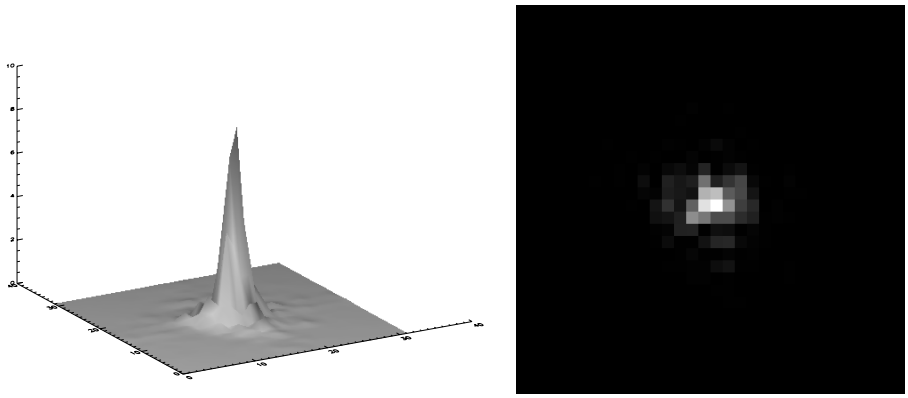

Figure I.1.2: Image spot at the focal of a lenslet, in presence of atmospherical turbulence, $d/r_0 = 2$. The subaperture is square with a FoV of 16×16 λ/d. There is no noise.

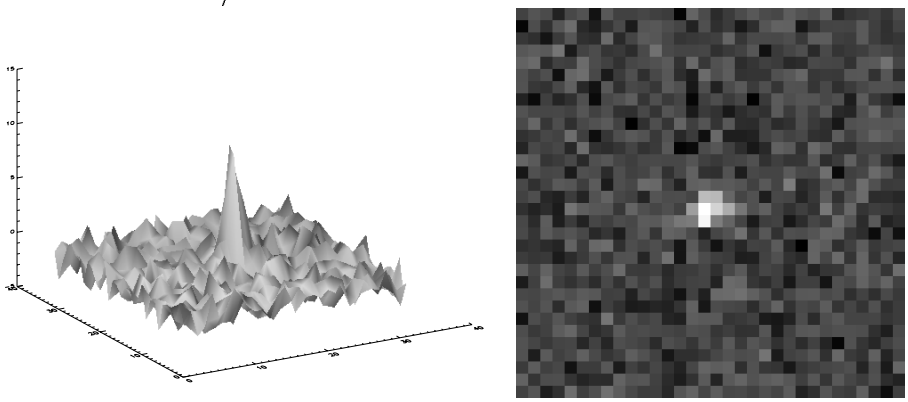

Figure I.1.3: Image spot at the focal of a lenslet, in presence of atmospherical turbulence, $d/r_0 = 2$, readout noise ($N_r = 1$) and photon noise. The subaperture is square with a FoV of 16×16 λ/d and the flux per subaperture and frame is 100 photons.

where α is the response coefficient, f_{nl} the non-linearity function of the considered algorithm and ϵ the errors due to the spot shape. The term $noise$ corresponds to photon noise and readout noise. We then write:

$$\sigma^2_{\Delta\Phi} = \left\langle [(\alpha - 1)D_x + f_{nl}(D_x) + \epsilon + bruit]^2 \right\rangle \tag{I.1.3}$$

$f_{nl}(x)$ can be defined by the Taylor derivation around D_x. The constant and the linear terms are by definition null. Moreover, we assume that $f_{nl}(x)$ is symmetric against $x = D_x$, leading to a null quadratic term. Thus we can approach it by:

$$f_{nl}(D_x) \approx \beta D_x^3, \tag{I.1.4}$$

where β is the cubic coefficient.

It is logical to assume that the photon noise and the readout noise are not correlated to the spot shape and position. Also we have $\sigma^2_{noise} = \langle [noise]^2 \rangle$ equal to the sum of two terms $\sigma^2_{\Delta\Phi,N_r}$ and $\sigma^2_{\Delta\Phi,N_{ph}}$. Other less obvious assumptions are made: 1) ϵ and D_x are not correlated and 2) α is constant (which is true for Gaussian spots or if there is no atmospherical turbulence i.e. $d/r_0 < 1$). Finally, the response coefficient α has been adjusted to 1. Equation I.1.3 then becomes:

$$\sigma_x^2 = \sigma^2_{\Delta\Phi,N_r} + \sigma^2_{\Delta\Phi,N_{ph}} + \beta^2 \left\langle D_x^6 \right\rangle + \left\langle \epsilon^2 \right\rangle . \tag{I.1.5}$$

I.1.2.3 Link between simulation and theory

The final *parameter* is the error variance $(\sigma_{err})^2$ given in $pixels^2$. Most of the graphs in this report show the phase error variance $(\sigma_{\Delta\phi})^2$ in radians^2 versus the photon noise. The link between the two variances is:

$$\sigma^2_{\Delta\phi} = \sigma^2_{err} * (2\pi/N_{samp})^2 . \tag{I.1.6}$$

This relationship results from the definition of the phase difference ϕ for a motion of one pixel at the lenslet array:

$$\phi = \frac{2\pi}{\lambda} * \delta_{opd}, \tag{I.1.7}$$

where δ_{opd} is the optical difference (OPD) $\delta_{opd} = \alpha_{pix} d$, where α_{pix} is the incoming angle shown on Fig. I.1.4. For a sampling of the diffraction spot equal to N_{samp}, $\alpha_{pix} = (\lambda/d)/N_{samp}$. Therefore, 1 pixel on the detector correspond to a phase difference of ϕ:

$$\phi = \frac{2\pi}{\lambda} \frac{\lambda}{d} \frac{1}{N_{samp}} d = \frac{2\pi}{N_{samp}} \tag{I.1.8}$$

We give in this report the error variance of the phase ϕ. Often in the literature, one gives the error variance of the incoming angle (α) either in CCD pixels or in arcsec. Those two parameters are linked by:

$$\sigma^2_{err} = \sigma^2_{\Delta\phi} * \left(\frac{N_{samp}}{2\pi} \right)^2 \ pixels^2, \quad \sigma^2_{\alpha} = \sigma^2_{\Delta\phi} * \left(\frac{\lambda/d}{2\pi} \right)^2 \ rad^2 \tag{I.1.9}$$

For example, if $N_{samp} = N_T = 2.355\sigma$, $\sigma^2_{err} = 1$ pixel corresponds to $\sigma_{\Delta\Phi} = 2\pi/2.355 = 2.67$ rad, and therefore to a phase error variance of 7.1 rad^2.

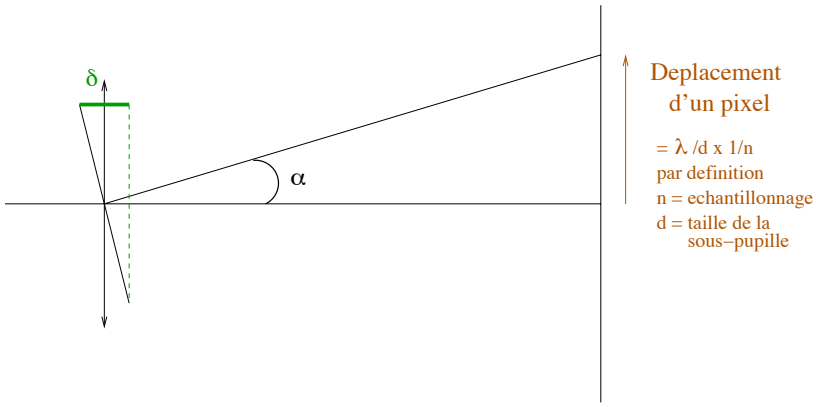

Figure I.1.4: Relationship between the spot motion in pixels and the slope of the wavefront in radians.

I.1.3 Algorithms

I.1.3.1 "Direct" methods

"Direct" methods are the ones used to directly process the image itself. I will consider here the center of gravity (CoG), the thresholding, the windowing, the weighted center of gravity (WCoG) and the quad cell (QC). The goal is to consider in the measurement only pixels with signal. The problem comes from the fact that usually those methods depend on the detection of the maximum position and thus are not reliable a low flux. For the windowing and the WCoG, one solution is to keep the window fixed introducing however some truncation noise.

The simple CoG

The CoG is the intrinsic way to calculate the position of a spot. Given an image of size $N \times N$ corresponding to a subaperture, with the intensity repartition $I_{x,y}$, the center of mass $(C_{mes})_x$, is:

$$(C_{mes})_x = \frac{\sum_{x=-N/2}^{N/2} \sum_{y=-N/2}^{N/2} I_{x,y} \times x}{\sum_{x=-N/2}^{N/2} \sum_{y=-N/2}^{N/2} I_{x,y}}, \tag{I.1.10}$$

This approach is at the same time very precise (especially for high SNR) and easy to implement, explaining why it is broadly used in AO. However, this method is not optimal because of the amplification of the noise for the pixels on the edge.

Analytical expression.

The analytical expression of the error variance in presence of readout noise and photon noise have been introduced by G. Rousset [Rousset, 1999]. The readout noise is a Gaussian noise centered and uniform while the photon noise is poissonian. The formula have been derived in the case of a Gaussian and Nyquist sampled spot.

$$\sigma^2_{\Delta\phi,N_r} = \frac{\pi^2}{3} \frac{N_r^2}{N_{ph}^2} \frac{N_s^4}{N_{samp}^2} \text{ radians}^2 \text{ readout noise} \tag{I.1.11}$$

$$\sigma^2_{\Delta\phi,N_{ph}} = \frac{\pi^2}{2ln2} \frac{1}{N_{ph}} \left(\frac{N_T}{N_{samp}} \right)^2 \text{ radians}^2 \text{ photon noise.} \tag{I.1.12}$$

where N_T is the FWHM of the image spot in pixels, N_s^2 is the total number of pixels used in the calculation and $N_{samp} = (\lambda/d)/p$, where p is the pixel size in rad. I used this definition for N_{samp} even for a Gaussian spot since this function is a first approximation of the diffraction spot. By

definition, I consider a Gaussian function of FHWM equal to $N_{samp} = \lambda/d$. This approximation is in some cases to brutal and it will be better to consider directly the diffraction limited spot, for which the intensity repartition is a $sinc^2$ function. However, the formula I.1.11 are not always validIn both cases, $N_T = N_{samp}$.

In theory, the CoG method is linear with a response coefficient equal to 1. In practice, the detectors are of finite sizes, which leads to a bias as well as possible non-linearity. For a Gaussian spot of rms size σ and centered on $(D_x, 0)$, the expression of the center of mass, $(C_{mes})_x$ calculated over a window W is [Fusco et Nicolle, 2005]:

$$(C_{mes})_x = D_x - \sigma \sqrt{\frac{2}{\pi}} \frac{e^{-A^2} - e^{-B^2}}{\Phi(B) + \Phi(A)}, \tag{I.1.13}$$

where $\Phi(t) = \frac{2}{\sqrt{\pi}} \int_0^t e^{-u^2}\, du$, $A = \frac{W/2 - D_x}{\sigma\sqrt{2}}$ et $B = \frac{W/2 + D_x}{\sigma\sqrt{2}}$
The comparison between simulation and theory (Eq. I.1.13) is very good.

Moreover, if $W/2 > 2\sqrt{2}\sigma$, true only if D_x is small ($D_x \ll 1$), then:

$$C_x \simeq D_x - \sigma_{spot} \sqrt{\frac{2}{\pi}} e^{-\frac{(W/2)^2}{2\sigma_{spot}^2}} \left[\frac{W_{D_x}}{\sqrt{2}\sigma_{spot}} + \frac{1}{6} \left(\frac{W_{D_x}}{\sqrt{2}\sigma_{spot}} \right)^3 \right] \tag{I.1.14}$$

This equation can be written as the sum of two terms: the response coefficient and the non-linearity coefficient:

$$(C_{mes})_x \simeq \underbrace{\left(1 - \sigma\sqrt{\frac{2}{\pi}} e^{-\frac{(W/2)^2}{2\sigma^2}}\right)\left(\frac{W}{\sqrt{2}\sigma}\right)}_{\alpha} D_x - \underbrace{\frac{1}{6}\left(\frac{W}{\sqrt{2}\sigma}\right)^3}_{\beta} D_x^3 \tag{I.1.15}$$

Note that α is close to 1. The deviation from 1 is less than 2.5 % for a $2\lambda/D$ window size and is less than 0.04 % for a 3 λ/D window size.

Windowing

This method consists in reducing the size of interest region on the detector before applying the CoG, disregarding the pixels on the edges that do not a priori have information on the signal.

There are two ways of using the windowing: with a fixed window or a mobil window. For the fixed window, the region is a square box of size $W \times W$ pixels centered on the FoV. For a mobil window, the region is a circular box of diameter W centered on the pixel of maximum intensity (D_x, D_y) (c.f. I.1.5). In both cases, the pixels located outside the box are set to zero. There is a significative difference between the two methods: the window is not centered on the same place: for the fixed window, the center is the center of the subaperture, at the intersection of 4 pixels while for a mobil window the center is a pixel (c.f. Fig I.1.5).

In the case of a mobil window one needs to know the approximate position of the spot which is harder to get when the SNR is low.

Thresholding

For this method, the threshold is first calculated by either taking a percentage T of the maximum when the SNr is high enough or by using the readout noise – for example 2^*N_r – for low SNR.

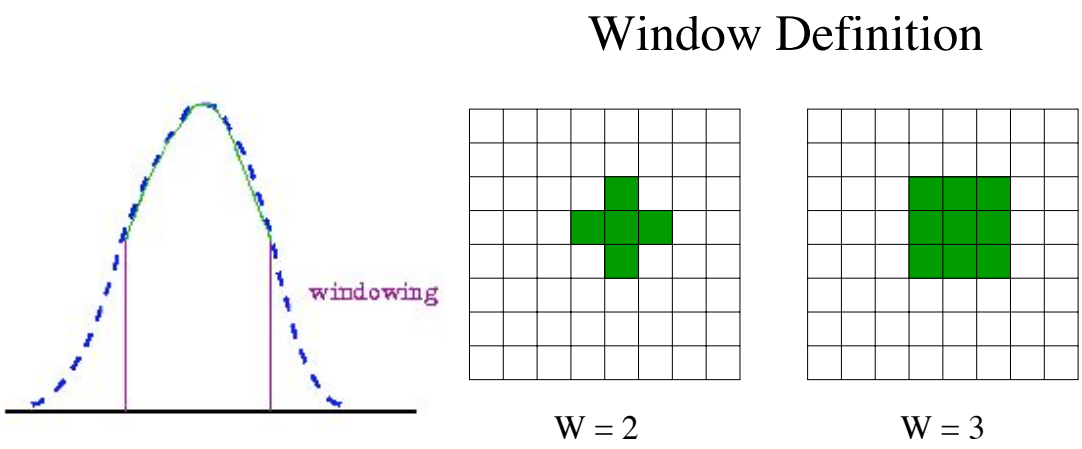

Figure I.1.5: Windowing. The two graphs describe the choice of the pixels in the case of a mobil window.

Once the threshold defined, there are two ways to actually threshold, as shown on Fig. I.1.6. In the first method, (c.f. Fig. I.1.6-I), the threshold is subtracted to the image and the pixels with negative intensity values are set to zero before using the CoG. In the second method (c.f. Fig I.1.6-II), the threshold is not subtracted, the pixels with intensity values less than the threshold are set to zero.

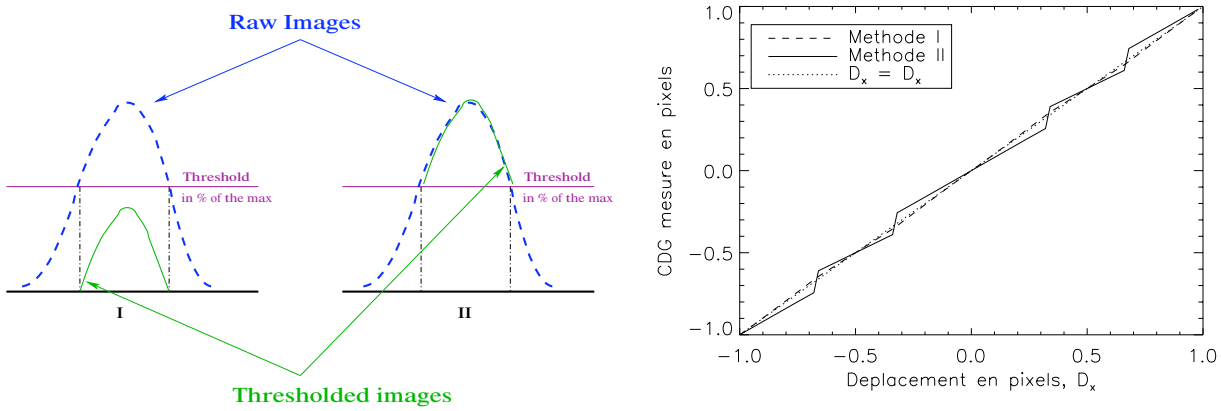

Figure I.1.6: Thresholding. On the left: illustration of the two thresholding methods I and II. $T = 0.1$. On the right: linearity of the two methods. In the simulation we will use method I.

The thresholding I is more reliable since linear. Indeed, let $I(x,y)$ be the intensity at the pixel (x,y) and $I'(x,y)$ the thresholded intensity such as $I'(x,y) = I(x,y) - s$, where s is the threshold value. The center of mass calculated on the domain N^2 of the non null pixels is for both cases I and II:

$$\begin{cases} I: & [(C_{mes})_x]_I = \frac{\sum I'(x,y)x}{\sum I'(x,y)} \\ II: & [(C_{mes})_x]_{II} = \frac{\sum I(x,y)x}{\sum I(x,y)} = \frac{\sum (I'(x,y)x + sx)}{\sum I'(x,y) + s} = \frac{\sum I'(x,y)x}{\sum I'(x,y) + N_S^2 * s} \end{cases} \quad \text{(I.1.16)}$$

Fig I.1.6-right shows the center of mass measured versus the true position of the spot for thresholding I and II. It is obvious that the method II introduces a bias, which is confirmed by eqs. I.1.16. The bias α is equal to:

$$\alpha = \left[1 + \frac{N_S^2 * s}{\sum I'(x,y)}\right]^{-1}. \quad \text{(I.1.17)}$$

Comments on the windowing and thresholding.

The thresholding and the windowing in the case of a mobil window depend on the direct detection of the maximum and are therefore very sensitive to noise and not very reliable at low SNR. But they are fast, easy to implement, and reliable for a medium SNR (such as a readout noise of 3 per pixel and a number of photon equal to 100 per subaperture).

The quad cell (QC)

The QC is a particular case of windowing where the size of the window is 2×2 pixels, in order to reduce the number of pixel to the minimum needed. There is a difference in the center of mass calculation, which will have its importance in the following:

$$(C_{mes})_x = \gamma \frac{\sum_i I(0 : N/2-1, i) - \sum I(N/2 : N-1, i)}{\sum I} \tag{I.1.18}$$

where γ is in pixels and is related to the response coefficient.

The QC has different advantages: it is fast computationally and it reduced the noise propagation, which explain its use in astronomy because it is often that we work with low fluxes with noisy detectors [Herriot, 2000] and the dominant error is due to the noise. However, it is not optimal for the new generation of CCD with low readout noise and new laser guide star. For those cases, the noise is not limiting the WFS error and the QC is not optimum since we lose in precision.

Moreover, because of γ, the performances of the QC depend on the determination of the size of the spot as well as its shape. In presence of big motions of the spot on the CCD – for high atmospherical turbulence in open loop for example – , a saturation occurs [Hardy, 1998]. The error due to the saturation if the dominant ones at high flux (c.f. figure I.1.7).

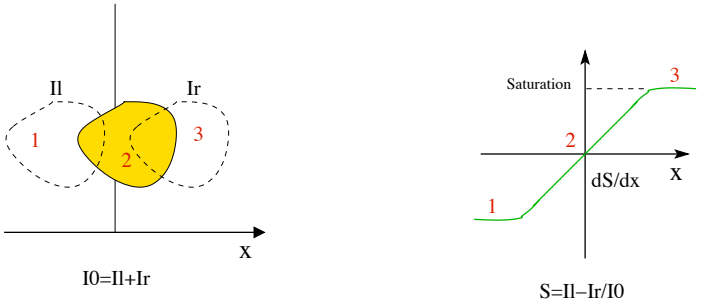

Figure I.1.7: Left: illustration of a spot on the QC. Right: Linearity curve that shows the saturation when the spot is displaced more than half its size. $S = (C_{mes})_x$

Calculation of γ for a Gaussian spot

The center of mass is $(C_{mes})_x = (I_l - I_r)/I_0$, where

$$I_l = \int_{-\infty}^{+\infty}\int_{-\infty}^{0} I(x,y)dxdy = \int_{-\infty}^{0} J(x)dx \ , \ I_r = \int_{-\infty}^{+\infty}\int_{0}^{+\infty} I(x,y)dxdy = \int_{0}^{+\infty} J(x)dx, \tag{I.1.19}$$

$$where \ \ J(x) = \int_{-\infty}^{+\infty} I(x,y)dy \tag{I.1.20}$$

Since the spot is Gaussian,
$I(x,y) = I(x)I(y)$ avec $I(x) = \frac{1}{\sqrt{2\pi\sigma^2}} e^{-x^2/2\sigma^2}$, $I(y) = \frac{1}{\sqrt{2\pi\sigma^2}} e^{-y^2/2\sigma^2}$.

To be sure the response is not biased, $\partial(C_{mes})_x/\partial x = 1$ (c.f. figure I.1.7). From the equations I.1.19, γ is equal to:

$$\gamma = \frac{I_0}{\partial Il/\partial x - \partial Ir/\partial x} = \frac{1}{2 * J(0)} = \frac{\sqrt{\pi}\sigma}{\sqrt{2}} \tag{I.1.21}$$

We will use this expression of γ as first approximation in the case of a spot distorted by the atmospherical turbulence. The difficulty will be to determine the value of σ.

Theoretical formula

For the QC, Eqs. I.1.11 become:

$$\sigma^2_{\Delta\phi,N_r} = \kappa^2 4\pi^2 \frac{N_r^2}{N_{ph}^2} \text{ radians}^2 \text{ readout noise} \tag{I.1.22}$$

$$\sigma^2_{\Delta\phi,N_{ph}} = \kappa^2 \frac{\pi^2}{2}\frac{1}{N_{ph}} \text{ radians}^2 \text{ photon noise.} \tag{I.1.23}$$

Pour une tache gaussienne, κ dépend de sa taille rms. Si l'on considère que la taille rms σ de la tache est donnée en radian (pour ce cas uniquement), on trouve que $\kappa = \gamma\ 2\pi/(\lambda/d) = \sqrt{2\pi}\ \sigma/(\lambda/d)$. Dans le cas d'une tache de diffraction, κ est égal à 1 [Rousset, 1999].

The weighted center of gravity (WCoG)

For the weighted center of gravity (WCoG) each pixel is associated to a different weight depending on its position on the CCD, thus its SNR. The contribution of the noisy pixels with low signal – like the one outside the spot – is attenuated. This method has been described and studied by [Nicolle et al., 2004]. The choice of the weighted function $P(x, y)$ is therefore important and depends on the SNR and the turbulence.

$$\hat{x}_{WCoG} = \frac{\sum xIx, y)P(x, y)}{\sum I(x, y)P(x, y)}. \tag{I.1.24}$$

The simplest case is when $P(x, y) = 1$ for $\sqrt{x^2 + y^2} < r$, which is the simple windowing. In the following I will use a Gaussian function with a FWHM N_w.

Nicolle et al. [2004] derived the theoretical formula of the phase error variance:

$$\sigma^2_{\Delta\phi,N_r} = \alpha^{-1}\frac{\pi^3}{32(ln2)^2}\frac{N_r^2}{N_{ph}^2}\frac{(N_T^2 + N_w^2)^2}{N_{samp}^2}\ radians^2,\ readout\ noise \tag{I.1.25}$$

$$\sigma^2_{\Delta\phi,N_{ph}} = \alpha^{-1}\frac{\pi^2}{2ln2}\frac{1}{N_{ph}}\left(\frac{N_T}{N_{samp}}\right)^2\frac{N_T^2 + N_w^2}{2 * N_T^2 + N_w^2}\ radians^2,\ photon\ noise. \tag{I.1.26}$$

where α is the response coefficient. This coefficient has to be considered to have a non-biased measure of the position. It is possible to calculate this coefficient as well as the non-linearity coefficient, β following the same method as for the simple CoG:

$$(C_{meas})_x = \left(\frac{\sigma_{\mathcal{W}}^2}{\sigma^2 + \sigma_{\mathcal{W}}^2}\right) D_x - \sigma_{eq}\sqrt{\frac{2}{\pi}}\frac{e^{-C^2} - e^{-D^2}}{\Phi(D) + \Phi(C)} \tag{I.1.27}$$

where σ_{eq} is defined as $\frac{1}{\sigma_{eq}^2} = \frac{1}{\sigma^2} + \frac{1}{\sigma_{\mathcal{W}}^2}$, where $\sigma_{\mathcal{W}}^2$ is the rms size of $P(x, y)$. Moreover, $C = \frac{W/2 - D_x}{\sigma_{eq}\sqrt{2}}$ et $D = \frac{W/2 + D_x}{\sigma_{eq}\sqrt{2}}$.

A first approximation gives

$$\alpha = \frac{\sigma_{\mathcal{W}}^2}{\sigma^2 + \sigma_{\mathcal{W}}^2} = \frac{N_{\mathcal{W}}^2}{N_T^2 + N_{\mathcal{W}}^2} \tag{I.1.28}$$

In the following, I consider that all the measure are corrected from this response coefficient α. The validity domain is similar to the CoG one.

It is worth mention that like the windowing, we can consider a weighting function centered on the center of the FoV or centered on the pixel with the maximum intensity. In this report, I only considered the fixed weighting function.

I.1.3.2 The indirect methods: the correlation

This method is not new and has been studied in [Poyneer et al., 2003], [Michau et al., 1992], and [Noël, 1997]. The hardest part in the calculation of the correlation peak position.

Correlation calculation

The noisy image obtained at the focal plane of the lenslet array is correlated with the reference image. The reference function is an approximation of the image without any noise. This is therefore a Gaussian function with FWHM N_w. This appears to be optimal in presence of readout noise. If the photon noise dominate, the optimal reference function is the logarithmic of the Gaussian function. However, the difference was not significant enough to be worth the complication of computation in this study.

By definition, the correlation function $I_c(x,y)$ of $I(u,v)$ by the reference function $P(u,v)$ is:

$$I_c(x,y) = \sum_{u=-N_c/2}^{N_c/2} \sum_{v=-N_c/2}^{N_c/2} I(u,v)P(u+x,v+y), \tag{I.1.29}$$

where N_c is the size of the matrix used in the calculation of the correlation. We need $N_c \geq 2N_{tot}$ to avoid truncation effect. It is simpler to calculate the correlation function in the Fourier domain since one property f the Fourier transform: the Fourier transform of a correlation of two functions is equal to the product of the Fourier transform of each function, one being conjugated.

$$I_c(x,y) = TF^{-1}[TF(I(x,y)) \times TF^*(P(x,y))], \tag{I.1.30}$$

where $(x,y) \in [0:2N_{tot}, 0:2N_{tot}]$.

Using the Fourier transform, it is possible to over-sample the correlation function. The Fourier transform of each function is put in a matrix of size $2*n \times N_{tot}$ before computing the inverse Fourier transform.

The choice of the reference FHWM is also a parameter. To optimize it, I introduced K_s such as $N_w = K_s N_{samp}$.

Using the correlation algorithm improves the contrast and reaches a better stability for lower SNR. However, the computation time might be a limitation for big telescopes. Moreover, it can be shown theoretically that the correlation should give us the best results in term of maximum-likelyhood. For a point source, this advantage appear to be low. However, it will become important for extended sources.

All this looks appealing. However, there is a problem of peak determination. Indeed, there are different ways to proceed: one can use the thresholding or windowing, parabola fitting or Gaussian fitting.

Peak determination

Simple CoG The easiest way is here again to use the simple CoG defined earlier (Eq. I.1.10) with $N_c \times N_c$ the size of the matrix used for the correlation calculation and $(I_c)_{x,y}$ the value of the

correlation function at the pixel. This method is obviously not optimal for the same reason as the ones given above.

Windowing: as described earlier, we only consider a central part of the correlation function to calculate the CoG. Only a fixed window has been studied.

Thresholding: it gives an unbiased calculation of the correlation peak. When the SNR is low, it the threshold needs to be increased. Similarly to the direct thresholding of the image, we define T_{corr} as the percentage of the maximum such as the threshold be $T_{corr} * max(I_c)$. The image used for the calculation of the CoG is defined as $(I_{res} = (I_c - T_{corr} * max(I_{ini})) > 0)$.

To be able to increase the threshold to get the optimal performances, we use the oversampling method described earlier. If the correlation function is not over-sampled, the thresholding level will be limited.

Parabola fitting This method has been described by Lisa Poyneer [Poyneer et al., 2003] and Vincent Michau. The goal is to fit the correlation function with a parabola, only close to the maximum.

If x_n is a number of points associated to a value I_n, and $n \geq 3$, we can define a parabola $f(x)$ such as $f(x) = a + bx + cx^2$. a,b and c are calculated to minimize:

$$\sum_{i=1}^{n} [I_i - f(x_i)]^2 = \sum_{i=1}^{n} \left[I_i - (a + bx_i + cx_i^2)\right]^2 \tag{I.1.31}$$

Solving this system is equivalent to put the derivative by a, b, and c to zero, leading to:

$$\begin{cases} (E1): & \sum_{i=1}^{n} [I_i] = a \sum_{i=1}^{n} [1] + b \sum_{i=1}^{n} [x_i] + c \sum_{i=1}^{n} [x_i^2] \\ (E2): & \sum_{i=1}^{n} [x_i I_i] = a \sum_{i=1}^{n} [x_i] + b \sum_{i=1}^{n} [x_i^2] + c \sum_{i=1}^{n} [x_i^3] \\ (E3): & \sum_{i=1}^{n} [x_i^2 I_i] = a \sum_{i=1}^{n} [x_i^2] + b \sum_{i=1}^{n} [x_i^3] + c \sum_{i=1}^{n} [x_i^4] \end{cases}$$

Let's be x_0, I_0 the position and value of the maximum and x_i, I_i the position and value of the pixel i. Resolving the system {(E1),(E2),(E3)} allows to find the parameters a, b et c and calculate the peak position, $X_c = x_0 - b/2c$.

Let's consider x_{-1}, x_0 et x_1, then:

$$X_c = x_0 - 0.5 * \frac{I_1 - I_{-1}}{I_1 + I_{-1} - 2I_0}. \tag{I.1.32}$$

This development has been done in one dimension (1D) and we are working with two dimensions images (2D). To use the formula, we first found the maximum (x_m, y_m) and then applied the equation I.1.33 to $(x_0 - 1, y_0)$, (x_0, y_0), $(x_0 + 1, y_0)$ to find the peak in the X-coordinate and similarly for the Y-coordinates (c.f. Fig. I.1.8).

$$X_c = x_0 - 0.5 * \frac{I(x_1, y_0) - I(x_{-1}, y_0)}{I(x_1, y_0) + I(x_{-1}, y_0) - 2I(x_0, y_0)}. \tag{I.1.33}$$

Gaussian fitting We used the function *Gaussfit* in IDL[1] to compute the fitting of the correlation function by a Gaussian. Here again we needed to work at 1D, and worked therefore on lines and

[1]Interactive Data Language, software

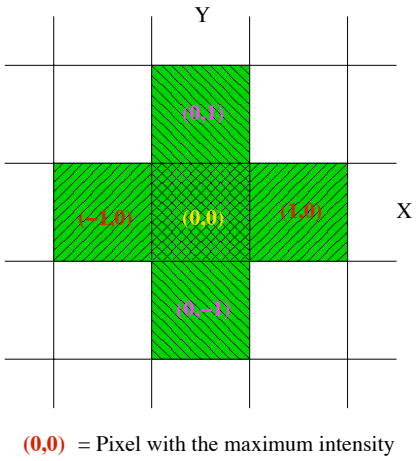

Figure I.1.8: Pixels used in the peak determination by the parabola fitting method.

columns separately.

For this method, we will first compare the 4 methods of peak correlation. The main result is that all methods are more or less equivalent except the widowing which introduces non-linearity.

Theoretical variance

Theoretical formula of the error variance have been developed with Vincent Michau in presence of readout noise [Michau, 2005] and for the thresholding method. Let's s be the threshold and D the domain for which $I_c(x,y) \geq s$, and D_c is the domain on which the function are defined. The correlation peak is then:

$$x_{corr} = \frac{\int_D x\left[I_c(x,y)-s\right]dxdy}{\int_D \left[I_c(x,y)-s\right]\mathrm{d}x\mathrm{d}y} = \frac{N_g}{D_g} \tag{I.1.34}$$

We assume the reference function to be determinist and the denominator fluctuations negligible compared to the numerator ones. Then the error variance becomes:

$$\sigma^2_{x,corr} = \frac{\langle N_g^2\rangle - \langle N_g\rangle^2}{\langle D_g\rangle^2}, \tag{I.1.35}$$

where

$$\langle N_g^2\rangle - \langle N_g\rangle^2 = \int_D\int_D xx'\sigma^2_{I_c}(x,y,x',y')\mathrm{d}x\mathrm{d}y\mathrm{d}x'\mathrm{d}y', \tag{I.1.36}$$

where $\sigma^2_{I_c}(x,y,x',y')$ is the variance of the correlation function. We can show that:

$$\begin{aligned}\sigma^2_{I_c}(x,y,x',y') = \int_{D_c}\int_{D_c} P(u,v)P(u',v')\left[\langle I(u+x,v+y)I(u'+x',v'+y')\rangle\right.\\ \left.-\langle I(u+x,v+y)\rangle\langle I(u'+x',v'+y')\rangle\right]\mathrm{d}u\mathrm{d}v\mathrm{d}u'\mathrm{d}v'.\end{aligned} \tag{I.1.37}$$

But

$$\begin{aligned}\left[\langle I(x,y)I(x',y')\rangle - \langle I(x,y)\rangle\langle I(x',y')\rangle\right] =\\ \begin{cases}\sigma_b^2(x,y), & \text{if } (x,y)=(x',y')\\ 0, & \text{if } (x,y)\neq(x',y')\end{cases}\end{aligned} \tag{I.1.38}$$

where $\sigma_b(x,y)$ is the noise density. In presence of readout noise, white noise, σ_b is constant and equal to N_r. Then

$$\sigma_C^2(x,y,x',y') = N_r^2 \int_{D_c} P(u,v)P(u+x-x',v'+y-y')dudv \tag{I.1.39}$$

A development of Eq. I.1.35 gives:

$$\sigma_{N_r}^2 = N_r^2 \frac{\int_D \int_D xx' \left[C_{\langle P\rangle}(x-x',y-y')\right] dxdydx'dy'}{\langle D_g\rangle^2}, \tag{I.1.40}$$

where $C_{\langle P\rangle}$ is the autocorrelation of the function P. $\sigma_{N_r}^2$ is in pixels^2.

V. Michau developed a simplified expression of Eq. I.1.40 using that:

$$C_{\langle P\rangle}(x,y) \approx C_I(x,y)(D_c \otimes D_c)(x,y) \tag{I.1.41}$$

close to the maximum. This function can be fitted by a parabola close to the maximum such as:

$$C_I(x,y) = N_{ph}^2 \left(1 - \frac{x^2+y^2}{2\delta^2}\right) \tag{I.1.42}$$

where δ is the FWHM of $C_{\langle P\rangle}$.

Therefore,

$$\sigma_{N_r}^2 = \frac{4\delta^2 N_r^2}{N_{ph}^2}. \tag{I.1.43}$$

I.1.4 Program description

I.1.4.1 Shape of the spot

In this study I focussed on two types of sources:

- **A perfect flat wavefront** which gives a diffraction in the focal plane of the lenslet. As a first approximation, I consider the spot to be Gaussian. If D_x, D_y is the position of the center of gravity of the Gaussian then the intensity repartition on the detector is:

$$I(x,y) = \frac{N_{ph}}{2\pi\sigma^2} e^{-\frac{(x-D_x)^2+(y-D_y)^2}{2\sigma^2}}, \; avec \; N_{ph} = \int\int_{-\infty}^{+\infty} I(x,y)dxdy \tag{I.1.44}$$

  D_x and D_y are randomly defined using a Gaussian repartition of amplitude rms Dep_{amp}. In this report, I mainly chose $Dep_{amp} = 0.1$ pixel, equivalent to about 10% of the rms spot size for a Nyquist sampling. In some cases, the approximation of the diffraction spot by a Gaussian is not enough and it is needed to consider the $sinc^2$ function of the Airy disk:

$$I(x,y) = \mathrm{sinc}^2\left(\frac{xd}{p\lambda}\right) \mathrm{sinc}^2\left(\frac{yd}{p\lambda}\right), \tag{I.1.45}$$

  where $\mathrm{sinc}(y) = \sin(\pi y)/(\pi y)$ and $p = (\lambda/d)/N_{samp}$.

- **Turbulent wavefront**. In AO, we will more likely have on the CCD a spot distorted by the turbulence than a diffraction spot. The spot distortion depends on the ratio d/r_0: if $d/r_0 < 1$ the spot are close to be diffraction limited and the intensity can be described by Eq. I.1.45. If $d/r_0 > 3$, the spot maximum bursts into speckle.

To compute *phi*, I used the power spectrum of the phase, which is after propagation through all turbulent layers:

$$\Phi_\varphi(\boldsymbol{f}) = 0.0228 * (r_0)^{-5/3} * (f_{2D})^{-11/3}, \tag{I.1.46}$$

for a Kolmogorov statistics. f is the two-dimensionnal spatial frequency. To get the phase from this expression, we se the inverse Fourier transform:

$$\varphi(x,y) = TF^{-1}[\sqrt{\Phi_\varphi(\boldsymbol{f_{2D}})} * [\text{random}(x) + i\,\text{random}(y)])], \tag{I.1.47}$$

where random(X) is the random function. Then the intensity repartition $I(x,y)$ is given by Fourier transform:

$$I(x,y) = N_{ph}|TF[Pup * (\cos(\phi) + i\sin(\phi))]|^2, \tag{I.1.48}$$

where *Pup* is the pupil. In this case, the true centroid is the defined by the G-tilt:

$$D_x \propto \frac{1}{d^2}\int\int_{sous-pupille} \frac{\partial\phi}{\partial x}dxdy = \frac{1}{d}\int_0^d \phi(d,y)dy - \frac{1}{d}\int_0^d \phi(0,y)dy, \tag{I.1.49}$$

I.1.4.2 Reliability of the result and robustness

If we do not set limits, the program always calculate an error variance. However, this variance might be wrong especially when the SNR is low. To be sure to trust our data, I introduced some validity tests in the program.

Test on the maximum intensity of the image. This condition is useful to verify that the image is not dominated by the noise and to be sure we are considering some signal. I set this condition at the beginning of the data processing to be $max(I(x,y)) > 2 * N_r$.

Test on the error made. We assume that the measured center of mass can not be too far of the true value. Therefore, at each iteration we check that $(C_{mes})_{x/y} - D_{x/y}$ is less than $2 * \sigma$.

If one condition is not satisfied, the error for the iteration is set to zero and we increment a test variable *Nul*. If *Nul* reaches half of the iterations (500 in my program) the error variance is not considered and does not appear on the final graph.

Finally, a last test is made on the error variance itself. Again the error can not be too high and we set a higher limit for the variance equal to the rms size of the spot: $(\sigma_{err})^2 < \sigma^2$. In this study, the image is mainly Nyquist sampled, thus $(\sigma_{err})^2_{limite} \approx 7\ rad^2$ (c.f. Eq. I.1.9).

I.1.4.3 Program architecture

The program has first been developed to verify the theoretical formulae in the simple case of a Gaussian spot. Then we used a spot distorted by the atmospherical turbulence. The architecture and the logic of the program is given on Fig. I.1.9.

Batch.pro Program that defines the parameters that I want to vary:

- Choice of the source: Gaussian, diffraction limited ($sinc^2$) or limited by the turbulence
- N_{ph}: photon number per frame
- N_r: readout noise
- T et T_{corr}: % of the maximum to define the threshold value (on the direct image or the correlated function)
- N_w FWHM of the reference function

- K_s such as $N_w = K_s\sigma$
- n: over-sampling factor
- W: Window size

Main.pro This routine allocates the memory for the matrix and calls the following other routines:

PSF.pro Creation of the matrix with 1000 of PSF created by source.pro. We then add noise;

Source.pro PSF calculation depending on the choice of the source, without noise;

Centroid.pro Calculation of the CoG : calls the different routines depending on the choice of image processing;

Thres.pro Thresholding;

Win.pro Windowing and weighted CoG;

Corr.pro Correlation;

Quad.pro Quad Cell.

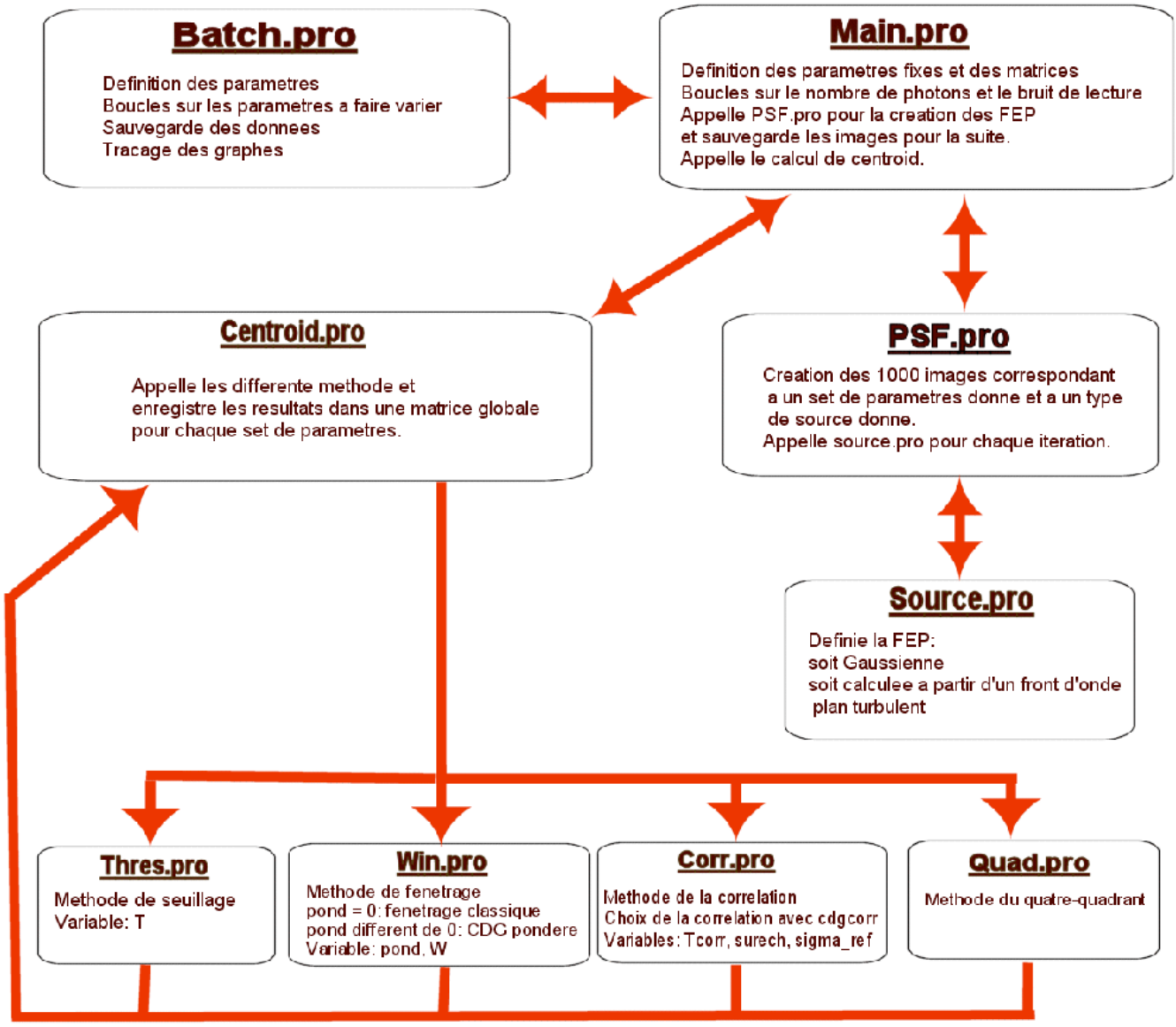

Figure I.1.9: Program architecture.

The number of iteration is 1000 per parameters. Also, unless stated, I considered well sampled images, $N_{samp} = 2$.

Table I.1.2 gives a summary of the methods and parameters studied as well as the figure related to it. The sign"-" means that the parameter does not exist for that box and the sign "**?**" means that I have not studied this set of method-parameter yet.

Table I.1.2: Summary

	Linearity	N_{samp}	**spot**	W_{fov} **ou** N_c	T **ou** T_{corr}	N_w	n
CoG	Fig. 12	Fig. 11	Gaussian:	Fig. 16	-	-	-
	Fig. 13		Diffraction:	Fig. 15	-	-	-
	Fig. 14		Atmosphere:	Fig. 32, 33	-	-	-
Threshold	Fig. 17	-	Gaussian:	Fig. 16	Fig. 18, 19	-	-
			Diffraction:	-	?	-	-
			Atmosphere:	-	Fig. 34	-	-
WCoG	Eq.29	Fig. 11	Gaussian:	Fig. 21, 22	-	?	-
			Diffraction:	Fig. 21, 22	-	?	
			Atmosphere:	Fig. 36, 37	-	Fig. 36	-
QC	Fig. 20		Gaussian:	-	-	-	-
			Diffraction:	-	-	-	-
			Atmosphere:	Fig. 35	-	-	-
Correlation windowing	Fig. 23		Gaussian:	Fig. 24	-	$= N_{samp}$	$= 1$
			Diffraction:	?	-	?	?
			Atmosphere:	?	-	?	?
Correlation threshold	Fig. 25	Fig. 10	Gaussian:	-	Fig. 26	Fig. 26	Fig. 27
			Diffraction:	-	?	?	?
			Atmosphere:	-	Fig. 40, 41	Fig. 39	$= 4$
Correlation parabola fitting			Gaussian:	-	-	N_{samp}	$= 2$
			Diffraction:	-	-	?	$= 2$?
			Atmosphere:	-	-	N_{samp}	$= 2$
Correlation Gaussian fitting	Fig. 28		Gaussian:	-	?	N_{samp}	$= 1$
			Diffraction:	-	?	?	$= 1$?
			Atmosphere:	-	?	N_{samp}	$= 1$

Table I.1.3 gives the summary of all the comparison done in between different methods.

Table I.1.3: Comparison of the results: Corr means comparison between different peak determination methods. All means comparison in between the different methods.

Gaussian	Corr	Fig. 29
Gaussian	All	Fig. 31
Atmosphere	Corr	Fig. 38
Atmosphere	All	Fig. 43, Fig. 44

Bibliography

Alves J. F., Lada C. J., Lada E. A., *Internal structure of a cold dark molecular cloud inferred from the extinction of background starlight*, Nature, Vol. 409, pp. 159-161, 2001

Angel R., Lloyd-Hart M, *Atmospheric tomography with laser bacons for correction of wide fields and 30-m class telescope*, Proc. SPIE, Vol. 4007, pp. 270-276, 2000.

Apai D., Pascucci I., Henning T., Sterzik M. F., Klein R., Semenov D., Günther E., Stecklum B., *Mid-infrared Observations of Brown Dwarfs and their Disks: First Ground-based Detection*, Proc. "The interaction of stars with their environment II.", ed: Kiss C, Kun M., Könyves V., pp. 93-98, 2003

Arines J., Ares J., *Minimum variance centroid thresholding*, Opt. Lett., Vol. 27, pp. 497-499, 2002

Athey A. E., Shectman S., Schechter P., Lane B., *The GMT ground-layer AO experiment at the Magellan telescopes*, Proc. SPIE, Vol. 5490, pp. 960-965, 2004

Bass M., *Handbook of optics*, sponsored by OSA, deuxième édition, Vol. 2, pp. 1995, 2001

Bate M. R., Bonnell I. A., Bromm V., *The formation of close binary systems by dynamical interactions and orbital decay*, MNRAS, Vol. 336, pp. 705-713, 2002a

Bate M. R., Bonnell I. A., Bromm V., *The formation mechanism of brown dwarfs*, MNRAS, Vol. 332, pp. L65-L68, 2002b

Bate M. R., Bonnell I. A., Bromm V., *The formation of a star cluster: predicting the properties of stars and brown dwarfs*, MNRAS, Vol. 339, pp. 577-599, 2003

Batten A.H., *Binary and multiple systems of stars*, Pergamon Press, Oxford, 1973

Beckers J. M., *Increasing the size of the isoplantétic patch with the multiconjugate adaptive optics*, Ed. Ulrich M.-H., ESO conference on very large telescopes and their instrumentation, Vol. 2, pp. 693-703, 1988

Blanc A., Fusco T., Hartung M., Mugnier L. M., Rousset G, *Calibration of NAOS and CONICA static aberrations. Application of the phase diversity technique*, A&A, Vol. 399, pp. 373-383, 2003

Bodenheimer P., *Angular Momentum Evolution of Young Stars and Disks*, ARA&A, Vol. 33, pp. 199-238., 1995

Bonnell I.A., *The formation of Close Binary Stars, The formation of Binary stars*, Ed. Zinneker H and Mathieu R.D., Proc. IAU, Vol. 200, pp. 23-32, 2001

Bonnell I. A., *A New Binary Formation Mechanism*, MNRAS, Vol. 269, pp. 837-848, 1994

Bonnell I. A., Bate M. R., Zinnecker H., *On the formation of massive stars*, MNRAS, Vol. 298, pp. 93-102, 1998

Bonnet H., Conzelmann R., Delabre B., Donaldson R., Fedrigo E., Hubin N., Kissler-Patig M., Lizon J-L., Paufique J., Rossi S., Stroebele S., Tordo S., *First light of SINFONI AO-module at VLT*, Proc. SPIE, Vol. 5490, pp. 130-138, 2004

Born M., Wolf E., *Principles of Optics*, Fifth Edition, Pergamon Press, New York, 1975

Boss A. P., *Gas Giant Protoplanet Formation: Disk Instability Models with Thermodynamics and Radiative Transfer*, ApJ, Vol. 563, pp. 367-373, 2001

Brandeker A., *T Tauri Multiple Systems*, Proc. IAU, Vol. 221, p.229, 2004

Burgasser A. J., Kirkpatrick J. D., Lowrance P. J., *Multiplicity among Widely Separated Brown Dwarf Companions to Nearby Stars: Gliese 337CD*, ApJ, Vol. 129, pp. 2849-2855, 2005

Butler D.J., Marchetti E., Bahr J., Xu W. and Hippler S., *Phase screens for astronomical multi-conjugate adaptive optics: application to MAPS*, Proc. SPIE, Vol. 4839, pp. 623-634, 2003

Charton J., Hubert Z., Stadler E., Schartz W., Beuzit J.-L., *System level simulation of micro-mirrors for adaptive optics*, Proc. SPIE, Vol. 4842, pp. 207-218, 2003

Close L. M., Siegler N., Freed M., Biller B., *Detection of Nine M8.0-L0.5 Binaries: The Very Low Mass Binary Population and Its Implications for Brown Dwarf and Very Low Mass Star Formation*, ApJ, Vol. 587, pp. 407-422, 2003

Conan J.M., *Etude de la correction partielle en Optique Adaptative*, Thèse de doctorat, Paris XI, 1994

Delgado-Donate E. J., Clarke C. J., Bate, M. R., *Accretion and dynamical interactions in small-N star-forming clusters: N= 5*, MNRAS, Vol. 342, pp. 926-938, 2003

Dicke R. H., *Phase-contrast detection of telescope seeing errors and their correction*, ApJ, Vol. 198, pp. 605-615, 1975

Duquennoy A., Mayor M., *Multiplicity among solar-type stars in the solar neighbourhood. II - Distribution of the orbital elements in an unbiased sample*, A&A, Vol. 248, pp. 485-524., 1991

Ellerbroek B. L., *First-order performance evaluation of adaptive optics systems for atmospheric turbulence compensation in extended field of view astronomical telescope*, App. Opt., Vol. 11, pp. 783-805, 1994

Ellerbroek B. L., Rigaut F., *Scaling Multi-Conjugated Adaptive Optics Performance Estimates to Extremely large telescopes*, Proc. SPIE, Vol. 4007, pp. 1088-1099, 2000

Ellerbroek B. L., Rigaut F. J., Bauman B. J., Boyer C., Browne S. L., Buchroeder R. A., Catone J. W., Clark P., d'Orgeville C., Gavel D. T., Herriot G., Hunten M. R., James E., Kibblewhite E. J., McKinnie I. T., Murray J. T., Rabaud D., Saddlemyer L. K., Sebag J., Stillburn J., Telle J. M., Veran J.-P., *Multiconjugate adaptive optics for Gemini-South*, Proc. SPIE, Vol. 4839, pp. 55-66, 2003

Esposito S., Feeney O., Riccardi A., *Laboratory test of pyramid wavefront sensor*, Proc. SPIE, Vol. 4007, pp. 416-422, 2000

Foy R., Labeyrie, A., *Feasibility of adaptive telescope with laser probe*, A&A, Vol. 152, pp. 129-131, 1985

Foy R., Migus A., Biraben F., Grynberg G., McCullough P. R., Tallon M., *The polychromatic artificial sodium star: a new concept for correcting the atmospheric tilt*, A&AS, Vol.111, p. 569, 1995

Fried D.L., *Statistics of a geometric representation of wavefront distortion*, JOSA, Vol. 55, pp. 1427-1435, 1965

Fried D.L., *Optical resolution through a randomly inhomogeneous medium for very long and very short exposures*, JOSA, Vol. 56, pp. 1372-1379, 1966a

Fried D.L., *Limiting resolution looking down through the atmosphere*, JOSA, Vol. 56, pp. 1380-1384, 1966b

Fried D.L., *Anisoplanatism in adaptive optics*, JOSA, Vol. 72, p. 52, 1982

Fusco T., Conan J.-M., Michau V., Mugnier L. M., Rousset G., *Phase estimation for large field of view: application to multiconjugate adaptive optics*, Proc. SPIE, Vol. 3763, pp. 125-133, 1999

Fusco T., *Correction partielle et anisoplanétisme en Optique Adaptative: traitement a posteriori et Optique Adaptative multiconjuguée*, Thèse de doctorat, ONERA, France, 2000

Fusco T., Conan J.-M., Rousset G., Mugnier L. M., Michau V., *Optimal wave-front reconstruction strategies for multiconjugate adaptive optics*, JOSA, Vol. 18, pp. 2527-2538, 2001

Fusco T., Rousset G., Rabaud R., et al., *NAOS on-line characterization of turbulence parameters and adaptive optics performance*, J. of Optics, Vol. 6, pp. 585-596, 2004

Fusco T., Rousset G., Beuzit J.-L., Mouillet D., Dohlen K., Conan R., Petit C., Montagnier G., *Conceptual design of an extreme AO dedicated to extra-solar planet detection by the VLT-Planet Finder instrument*, Proc. SPIE, Vol. 5903, pp. 148-159, 2005

Fusco T., Nicolle M., communication privée, ONERA, 2005

Gardner C.S., Voelz D.G., Sechrist C.F., Jr, Segal A.C., *Lidar studies of the nighttime sodium layer over Urbana, Illinois: 1. Seasonal and nocturnal variations*, J. Geophys. Res., Vol. 91, pp. 13659-13673, 1986

Gendron E., Léna P., *Astronomical Adaptive Optics. I. Modal control optimization*, A&A, Vol. 291, pp. 337-347, 1994

Gizis J. E., Kirkpatrick J. D., Burgasser A., Reid I. N., Monet D. G., Liebert J., Wilson J. C., *Substellar Companions to Main-Sequence Stars: No Brown Dwarf Desert at Wide Separations*, ApJ, Vol. 551, pp. L163-L166, 2001

Gonsalves R.A., *Phase retrieval and diversity in adaptive optics*, Opt. Eng., Vol. 21, pp. 829-832, 1982.

Grosso R.P., Yellin M., *The membrane mirror as an adaptive optical element*, JOSA, Vol. 67, p. 399, 1977 .

Halbwachs J. L., Arenou F., Mayor M., Udry S., Queloz D, *Exploring the brown dwarf desert with Hipparcos*, A&A, Vol. 355, pp.581-594, 2000

Hammer F., Puech M., Assemat F. F., Gendron E., Sayde F., Laporte P., Marteaud M., Liotard A., Zamkotsian F., *FALCON: a concept to extend adaptive optics corrections to cosmological fields*, Proc. SPIE, Vol. 5382, pp. 727-736, 2004

Hardy J.W., *Adaptive Optics for Astronomical Telescopes*, Oxford University Press, 1998

Hartung M., Blanc A., Fusco T., Lacombe F., Mugnier L. M., Rousset G., Lenzen R., *Calibration of NAOS and CONICA static aberrations. Experimental results*, A&A, Vol. 399, pp. 385-394, 2003

Hartung M, Lenzen R., Hofmann R., Bhm A., Brandner W., Finger G., Fusco T., Lacombe F., Laun W., Granier P., Storz C., Wagner K., *CONICA design, performance and final laboratory tests*, Proc SPIE, Vol. 4841, pp. 425-436, 2003b

Herriot G., Morris S., Anthon A. et al., *Progress on Altair: the Gemini North adaptive optics system*, Proc. SPIE, Vol. 4007, pp. 115-125, 2000

Hubin N. N., Le Louarn, M., Conzelmann R., Delabre B., Fedrigo E., Stuik R., *Ground layer AO correction for the VLT MUSE project*, Proc. SPIE, Vol. 5490, pp. 846-857, 2004

Hutchin R.A., *History and physical principles of Ledestar Technology*, Présentation donnée pour OSA, 1991, non publiée.

Irwan R., Lane R. G., *Analysis of optimal centroid estimation applied to Shack-Hartmann sensing*, Appl. Opt., Vol. 38, pp. 6737-6743, 1999

Jagourel P., Madec P.-Y. and Séchaud M., *Adaptives optics: a bimorph mirror for wavefront correction*, Proc. SPIE, Vol. 1271, pp. 160-171, 1990

Jayawardhana R., Ardila D. R., Stelzer B., Haisch K. E., *A Disk Census for Young Brown Dwarfs*, AJ, Vol. 126, pp. 1515-1521, 2003

Johnston D. C., Welsh B. M., *Analysis of multiconjugate adaptive optics*, JOSA, Vol. 11, pp. 394-408 , 1994

Kozai Y., *Secular perturbations of asteroids with high inclination and eccentricity*, AJ, Vol. 67, pp. 591-598, 1962

Keller Ch. U., Plymate C., and Ammons S.M., *Low-cost solar adaptive optics in the infrared*, Proc. SPIE, Vol. 4853, pp. 351-359, 2003

Kiseleva L. G., Eggleton P. P., Mikkola S., *Tidal friction in triple stars*, MNRAS, Vol. 300, pp. 292-302, 1998

Kokorowski S.A., *Analysis of adaptive optical elements made from piezoelectric bimorphs*, JOSA, Vol. 69, pp. 181-187, 1979

Kolmogorov A. N., *Local structure of turbulence in incompressible fluids with very high Reynolds number*, Dokl. Akab. Nauk. SSSR, Vol. 30, pp. 301-305, 1941

Kumar S. S., *The Structure of Stars of Very Low Mass*, ApJ, Vol. 137, pp. 1121-1125, 1963

Lada C. J., Lada E. A., *Embedded Clusters in Molecular Clouds*, ARA&A, Vol. 41, pp.57-115, 2003

Larson R. B., *The role of tidal interactions in star formation*, MNRAS, Vol. 332, pp. 155-164, 2002

Le Louarn M., *Étoiles laser pour les grands télescopes: effet de cône et implications astrophysiques*, thèse de doctorat, Université de Lyon, 2000a

Le Louarn M, Tallon M., *3D mapping of turbulence: theory*, Proc. SPIE, Vol. 4007, pp. 1066-1073, 2000

Le Louarn M., *Mutli-Conjugated Adaptive Optics with laser guide stars: performances in the infrared and visible*, MNRAS, Vol. 334, pp. 865-874, 2002

Le Louarn M., Hubin N., *Wide-field adaptive optics for deep-field spectroscopy in the visible*, MNRAS, Vol. 349, pp. 1009-1018, 2004

Le Roux B., Conan J.-M., Kulcsár C., Raynaud, H.-F., Mugnier L. M., Fusco T., *Optimal control law for classical and multiconjugate adaptive optics*, JOSA, Vol. 21, pp. 1261-1276, 2004

Liu M. C., Najita J., Tokunaga A. T., *A Survey for Circumstellar Disks around Young Substellar Objects*, ApJ, Vol. 585, pp. 372-391, 2003

Liotard A., Zamkotsian F., *Static and dynamic micro deformable mirror characterization by phase-shifting and time-averaged interferometry*, Proc. SPIE, Vol. 5494, pp. 480-491, 2004

Madec P.Y., *Control techniques*, "Adaptive optics in Astronomy", ed. F. Roddier, Cambridge University press, pp. 131-154, 1999

Marchetti E., Hubin N. N., Fedrigo E., Brynnel J., Delabre B., Donaldson R., Franza F., Conan R., Le Louarn M., Cavadore C., Balestra A., Baade D., Lizon J.-L., Gilmozzi R., Monnet G. J., Ragazzoni R., Arcidiacono C., Baruffolo A., Diolaiti E., Farinato J., Vernet-Viard E., Butler D. J., Hippler S., Amorin A., *MAD the ESO multi-conjugate adaptive optics demonstrator*, Proc. SPIE, Vol. 4839, pp. 317-328, 2003

Marcy G. W., Butler R. P., *Planets Orbiting Other Suns*, PASP, Vol. 112, pp. 137-140, 2000

Mayer L., Quinn T., Wadsley J., Stadel J., *Formation of Giant Planets by Fragmentation of Protoplanetary Disks*, Science, Vol. 298, pp. 1756-1759, 2002

Mathieu R., D., *Pre-Main-Sequence binary stars*, ARA&A, Vol. 32, pp. 465-530, 1994

McCall S.L., Passner A., *Adaptive optics in astronomy*, dans Adaptive optics and Short Wavelength, Addison-Wesley Pub., pp. 149-174., 1978

McDermid R, Bacon R., Adam G., Benn C., Cappellari M., *Adaptive-optics-assisted integral field spectroscopy with OASIS and NAOMI*, Proc. SPIE, Vol. 5492, pp. 822-829, 2004

McGlamery, *Computer simulation studies of compensation of turbulence degraded images*, Image processing, Vol. 74, pp. 225-233, 1976

Michau V., Rousset G., Fontanella J.C., *Wavefront sensing from extended sources*, dans real time and post facto solar image correction, Sunspot, New Mexico, USA 1992, NSO, pp. 124-128, 1992

Michau V., conversation privée, ONERA, 2005

Nakajima T., Oppenheimer B. R., Kulkarni S. R., Golimowski D. A., Matthews K., Durrance S. T., *Discovery of a Cool Brown Dwarf*, Nature, Vol. 378, p. 463, 1995

Nakajima T., *Signal-to-noise ratio of the bispectral analysis of speckel interferomatry*, JOSA, Vol. 9, pp. 1477-1491, 1988

Nicolle M., Fusco T., Rousset G., Michau V., *Improvement of Shack-Hartmann wavefront sensor measurement for Extreme Adaptive Optics*, Opt. Let., Vol. 29, pp. 2743-2745, 2004a

Nicolle M., Fusco T., Michau V., Rousset G., Blanc A., Beuzit J.-L., *Ground layer adaptive optics: analysis of the wavefront sensing issue*, Proc. SPIE, Vol. 5490, pp. 858-869, 2004b

Noël T., *Caractérisation spatiale et temporelle de la turbulence atmosphérique par analyse de front d'onde*, Thèse de doctorat, ONERA, France, 1997

Noll R.J., *Zernike Polynomials and atmospheric turbulence*, JOSA, Vol. 66, pp. 207-211, 1976

Obukhov A.M., *Structure of the temperature field in a turbulent current*, Izv. Akad. Nauk. SSSR, Ser. Geograf. Geofiz., Vol. 13, pp. 58-69, 1949

Olsen K. A., Blum R.D., Rigaut F., *Stellar Crowding and the Science Case for Extremely Large Telescopes*, ApJ, Vol. 126, pp. 452-471, 2003

Paschall R., Anderson D., *Linear Quadratic Gaussian control of a deformable mirror adaptive optics system with time-delayed measurements*, Appl. Opt., Vol. 32, pp. 6347-6358, 1993

Paxman R.G., Fienup J.R., *Optical misalignment sensing and image reoconstruction using phase diversity*, JOSA., Vol. 5, pp. 914-923, 1988

Paxman R.G., Schulz T.J., Fienup J.R., *Joint estimation of object and aberrations by using phase diversity*, JOSA, Vol. 9, pp. 1072-1085, 1992

Petit C., Quiros-Pacheco F., Conan J.-M., Kulcsár, Raynaud H.-F., Fusco T., et Rousset G., *Kalman filter based control loop for adaptive optics*, Proc. SPIE, Vol. 5490, pp. 1414-1425, 2004

Pilkington J. D. H., Thompson L., Gardner C., *Artificial Guide Stars for Adaptive Imaging*, Nature, Vol. 330, p. 116, 1987

Puech M., Sayede F., *FALCON: extending adaptive optics corrections to cosmological fields*, Proc. SPIE, Vol. 5492, pp. 303-311, 2004

Pourbaix D., Arenou F., *Screening the Hipparcos-based astrometric orbits of sub-stellar objects*, A&A, Vol. 372, pp.935-944, 2001

Poyneer L.A., LaFortune K., Awwal A.A.S., *Correlation wavefront sensing for Shack-Hartmann-based Adaptive Optics with a point source*, Lawrence Livermore National Lab Document September 2003 (Livermore, CA 94551), 2003

Ragazzoni R., *Pupil plane wavefront sensing with an oscillating prism*, J. Mod. Opt., Vol. 43, pp. 289-293, 1996

Ragazzoni R., Farinato J., *Sensitivity of a pyramidic wavefront sensor in closed loop adaptive optics*, A&A, Vol. 350, pp. L23-L26, 1999a

Ragazzoni R., *No Laser Guide Stars for adaptive optics in giant telescopes?*, A&AS, Vol. 136, pp. 205-209, 1999b

Ragazzoni R, Marchetti E., Valente G., *Adaptive-optics corrections available for the whole sky*, Nature, Vol. 403, pp. 54-56, 2000

Rebolo R., Magazzù A., Martín E. L., *Lithium and the Nature of Brown Dwarf Candidates*, Proc. ESO Workshop Held in Garching, eds. Tinney C. G., ESO Astrophysics Symposia, 1995

Reipurth B., Clarke C., *The Formation of Brown Dwarfs as Ejected Stellar Embryos*, ApJ, Vol. 122, pp. 432-439, 2001

Richardson E. H., Fletcher J. M., Morbey C. L., Oschmann J. M., Pazder J. S., *Optical design of Gemini ALTAIR*, Proc. SPIE, Vol. 3353, pp. 600-610, 1998

Rigaut F., Salmon D., Arsenault R., Thomas J., Lai O., Rouan D., Vran J. P., Gigan P., Crampton D., Fletcher, J. M., Stilburn J., Boyer C., Jagourel P., *Performance of the Canada-France-Hawaii Telescope - Adaptive Optics Bonnette*, PASP, Vol. 110, pp 152-164, 1998

Rigaut F., Ellerbroek B. L., Flicker R., *Principles, limitations, and performance of multiconjugate adaptive optics*, Proc. SPIE, Vol. 4007, pp. 1022-1031, 2000

Rigaut F., *Ground Conjugate Wide Field Adaptive Optics for the ELTs*, dans*Beyond conventional adaptive optics* Ed. by Vernet E., Ragazzoni R., Esposito S., et Hubin N. ESO Conf Workshop Proc., Vol. 58, pp.11-17, 2002

Robin A.C., Reyl C.,Derrire S., Picaud S., *A synthetic view on structure and evolution of the Milky Way*, A&A, Vol. 409, pp. 523-540, 2003, Erratum: A&A, Vol. 416, p. 157, 2004.

Roddier F., *The effect of atmospherical turbulence in optical astronomy*, Progress in Optics, ed. E.Wolf, Vol. XIX, pp. 281-376, 1981

Roddier F., Roddier C., *NOAO Infrared Adaptive Optics Program II: modeling atmospheric effects in adaptive optics systems for astronomical telescopes*, Proc. SPIE, Vol. 628, pp. 298-304, 1986

Roddier F. *Curvature sensing and compensation: a new concept in adaptive optics*, Appl. Opt., Vol. 27, pp. 1223-1225, 1988

Roddier N., *Atmospheric wavefront simulation using Zernike polynomials* Optical Engineering, Vol. 29, pp. 1174-1180, 1990

Roddier F., Anuskiewicz J., Graves J.E., Northcott M.J. et Roddier C., *Adaptive Optics at the University of Hawa I:Current performance at the telescope*, Proc. SPIE, Vol. 2201, pp. 2-9, 1994

Roddier F., *Adaptive Optics in Astronomy*, ed. Cambridge University Press, Cambridge, 1999a

Roddier F., *The UH-CFHT systems*, dans Adaptive Optics in Astronomy (Ref. Roddier [1999a]), Chap. 9, pp. 205-234, 1999b

Rousset G., Fontanella J.C., Primot J., Sève A., *Imagerie optique à travers la turbulence atmosphérique*, La Recherche Aérospatiale, Vol. 5, pp. 47-58, 1987

Rousset G., Lacombe F., Puget P, Hubin N. N., Gendron E., Conan J.-M., Kern P. Y., Madec P.-Y., Rabaud D., Mouillet D., Lagrange A.-M., Rigaut F. J., *Design of the Nasmyth adaptive optics system (NAOS) of the VLT*, Proc. SPIE, Vol. 3353, pp. 508-516, 1998

Rousset G., *Wavefront sensors*, dans Adaptive Optics in Astronomy [Roddier, 1999a], Chap. 5, pp 91-130, 1999

Rousset G., Lacombe F., Puget P., Gendron E., Arsenault R., Kern P. Y., Rabaud D., Madec P.-Y., Hubin N. N., Zins G., Stadler E., Charton J., Gigan P., Feautrier P., *Status of the VLT Nasmyth adaptive optics system (NAOS)*, Proc. SPIE, Vol. 4007, pp. 72-81, 2000

Ruggiu J.-M., Solomon C.J., Loos G., *Gram-Charlier matched filter for Shack-Hartmann sensing at low light levels*, Opt. Lett., Vol. 23, pp. 235-237, 1998

Sallberg S.A., Welsh B.M., Roggemann M.C., *Maximum a posteriori estimation of wave-front slopes using a Shack-Hartmann wave-front sensor*, JOSA, Vol. 14, pp. 1347-1354, 1997

Sandler D., *The design of laser beacon AO systems*, dans Adaptive Optics in Astronomy [Roddier, 1999a], Chap. 6, p. 294, 1999

Sasiela R.J., *Electromagnetic wavepropagation in turbulence*, Berlin: Springer-Verlag., 1994.

Sauvage J.-F., Fusco T. , Rousset G., Petit C. , Neichela B., Blanc A., Beuzit J.-L., *Fine calibration and pre-compensation of Non-Common Path Aberrations for high performance AO system*, Proc. SPIE, 2005, soumis.

Séchaud M., *Wave-front compensation device*, dans Adaptive Optics in Astronomy [Roddier, 1999a], Chap. 4, pp 57-90, 1999

Shack R.B. et Platt B.C., *Production and use of a lenticular Hartmann screen*, JOSA., Vol. 61, p.656, 1971

Shu F. H., Adams F. C., Lizano S., *Star formation in molecular clouds - Observation and theory*, ARA&A, Vol. 25, pp. 23-81, 1987

Smith N., Bally, J., Morse, J. A., *Numerous Proplyd Candidates in the Harsh Environment of the Carina Nebula*, ApJ, Vol. 587, pp. L105-L108, 2003

Steinhaus E., Lipson S.G., *Bimorph piezoelectric flexible mirror*, JOSA, Vol. 69, pp. 478-481, 1979

Sterzik M. F., Durisen R. H., Zinnecker H., *How do binary separations depend on cloud initial conditions?*, A&A, Vol. 411, pp. 91-97, 2003

Sterzik M. F., Durisen R. H., *Imprints of dynamical interactions on brown dwarf pairing statistics and kinematics*, A&A, Vol. 400, pp.1031-1042, 2003

Sterzik M. F., Durisen R. H., *Are Binary Separations related to their System Mass?*, Revista Mexicana de Astronoma y Astrofsica (Serie de Conferencias), Ed. Allen C. & Scarfe C., Vol. 21, pp. 58-62, 2004

Strehl K., Zeits. Instrum., Vol. 15, pp. 364, 1895

Strehl K., Zeits. Instrum., Vol. 22, pp. 214, 1902

Tallon M., Foy R., *Adaptive telescope with laser probe - Isoplanetism and cone effect*, A&A, Vol. 235, pp. 549-557, 1990.

Tassoul J.-L., *Theory of rotating stars*, Princeton Series in Astrophysics, Princeton: University Press, 1978

Tatarski V.I., *Wave Propagation In a Turbulent Medium*, Dover Publications, Inc. New York, Ed. R.A. Silverman, 1961

Thomas S., *A simple turbulence simulator for adaptive optics*, Proc. SPIE, Vol. 5490, pp. 766-773, 2004

Thompson L. A., Teare S. W., Crawford S. L., Leach R. W., *Rayleigh Laser Guide Star Systems: UnISIS Bow-Tie Shutter and CCD39 Wavefront Camera*, PASP, Vol. 114, pp. 1143-1149, 2002.

Tokovinin A. A., *MSC - a catalogue of physical multiple stars*, A&AS, Vol. 124, pp. 75-84, 1997a

Tokovinin A. A., *On the multiplicity of spectroscopic binary stars*, AL, Vol. 23, pp. 727-730, 1997b

Tokovinin A., Le Louarn M., Viard E., Hubin N., Conan R., *Optimized modal tomography in adaptive optics*, A&A, Vol. 378, pp. 710-721, 2001

Tokovinin A., Smekhov M. G., *Statistics of spectroscopic sub-systems in visual multiple stars*, A&A, Vol. 382, pp. 118-123, 2002

Tokovinin A., Kornilov V., Shatsky N., Voziakova O., *Restoration of turbulence profile from scintillation indices*, MNRAS, Vol. 343, pp. 891-899, 2003a

Tokovinin A., Baumont S., Vasquez J., *Statistics of turbulence profile at Cerro Tololo*, MNRAS, Vol. 340, pp 52-58, 2003b

Tokovinin, A., Gregory B., Schwarz H., Terebizh V., Thomas S., *A visible-light AO system for the 4.2m SOAR telescope*, Proc. SPIE, Vol. 4839, pp. 673-680, 2003

Tokovinin A., Thomas S., Gregory B., van der Bliek N., Schurter P., Cantarutti R., Mondaca E., *Design of ground-layer turbulence compensation with a Rayleigh beacon*, Proc. SPIE, Vol. 5490, pp. 870-878, 2004a

Tokovinin A., Thomas S., Vdovin G., *Using 50-mm electrostatic membrane deformable mirror in astronomical adaptive optics*, Proc. SPIE, Vol. 5490, pp. 580-585, 2004b

Tokovinin A., *Seeing Improvement with Ground-Layer Adaptive Optics*, PASP, Vol. 116, pp. 941-951, 2004c

Tokovinin A., Travouillon T., *Model of optical turbulence profile at Cerro Pachon*, MNRAS, submitted, 2005

van Dam M. A., Lane R. G., *Wave-front slope estimation*, JOSA, Vol. 17, pp. 1319-1324, 2000

Vernin J., Agabi A., Avila R., Azouit M., Conan R., Martin F., Masciadr E., Sanchez L., & Ziad A., 2000, in *Cerro Pachón and Cerro Tololo, Gemini RPT-AO-G0094, http://www.gemini.edu/.*

Winick K. A., *Cramer Rao lower bounds on the performance of Charge-Couple-Device optical position estimator*, JOSA(A), Vol. 3, pp. 1809-1815, 1986

Yaglom A.M., Doklady Akad. Nauk. SSSR, Vol. 69, p. 743, 1949.

Yellin M., *Using membrane mirrors in adaptive optics, Imaging Through the Atmosphere*, Proc. SPIE, Vol.75, p. 97, 1976

Zinnecker H., Mathieu R., *The Formation of Binary Stars*, Proc. IAU, 2001.

Zucker S., Mazer T., *Derivation of the Mass Distribution of Extrasolar Planets with MAXLIMA, a Maximum Likelihood Algorithm*, ApJ, Vol. 562, pp. 1038-1044, 2001

Gemini Ground Layer Adaptive Optics, Feasability report, http://www.gemini.edu/, 2005